Direct Evidence for Neutrino Flavor Transformation from Neutral-Current Interactions in the Sudbury Neutrino Observatory

Q.R. Ahmad,[17] R.C. Allen,[4] T.C. Andersen,[6] J.D. Anglin,[10] J.C. Barton,[11,*] E.W. Beier,[12] M. Bercovitch,[10] J. Bigu,[7] S.D. Biller,[11] R.A. Black,[11] I. Blevis,[5] R.J. Boardman,[11] J. Boger,[3] E. Bonvin,[14] M.G. Boulay,[9,14] M.G. Bowler,[11] T.J. Bowles,[9] S.J. Brice,[9,11] M.C. Browne,[17,9] T.V. Bullard,[17] G. Bühler,[4] J. Cameron,[11] Y.D. Chan,[8] H.H. Chen,[4,†] M. Chen,[14] X. Chen,[8,11] B.T. Cleveland,[11] E.T.H. Clifford,[14] J.H.M. Cowan,[7] D.F. Cowen,[12] G.A. Cox,[17] X. Dai,[11] F. Dalnoki-Veress,[5] W.F. Davidson,[10] P.J. Doe,[17,9,4] G. Doucas,[11] M.R. Dragowsky,[9,8] C.A. Duba,[17] F.A. Duncan,[14] M. Dunford,[12] J.A. Dunmore,[11] E.D. Earle,[14,1] S.R. Elliott,[17,9] H.C. Evans,[14] G.T. Ewan,[14] J. Farine,[7,5] H. Fergani,[11] A.P. Ferraris,[11] R.J. Ford,[14] J.A. Formaggio,[17] M.M. Fowler,[9] K. Frame,[11] E.D. Frank,[12] W. Frati,[12] N. Gagnon,[11,9,8,17] J.V. Germani,[17] S. Gil,[2] K. Graham,[14] D.R. Grant,[5] R.L. Hahn,[3] A.L. Hallin,[14] E.D. Hallman,[7] A.S. Hamer,[9,14] A.A. Hamian,[17] W.B. Handler,[14] R.U. Haq,[7] C.K. Hargrove,[5] P.J. Harvey,[14] R. Hazama,[17] K.M. Heeger,[17] W.J. Heintzelman,[12] J. Heise,[2,9] R.L. Helmer,[16,2] J.D. Hepburn,[14] H. Heron,[11] J. Hewett,[7] A. Hime,[9] J.G. Hykawy,[7] M.C.P. Isaac,[8] P. Jagam,[6] N.A. Jelley,[11] C. Jillings,[14] G. Jonkmans,[7,1] K. Kazkaz,[17] P.T. Keener,[12] J.R. Klein,[12] A.B. Knox,[11] R.J. Komar,[2] R. Kouzes,[13] T. Kutter,[2] C.C.M. Kyba,[12] J. Law,[6] I.T. Lawson,[6] M. Lay,[11] H.W. Lee,[14] K.T. Lesko,[8] J.R. Leslie,[14] I. Levine,[5] W. Locke,[11] S. Luoma,[7] J. Lyon,[11] S. Majerus,[11] H.B. Mak,[14] J. Maneira,[14] J. Manor,[17] A.D. Marino,[8] N. McCauley,[12,11] D.S. McDonald,[12] A.B. McDonald,[14,13] K. McFarlane,[5] G. McGregor,[11] R. Meijer Drees,[17] C. Mifflin,[5] G.G. Miller,[9] G. Milton,[1] B.A. Moffat,[14] M. Moorhead,[11] C.W. Nally,[2] M.S. Neubauer,[12] F.M. Newcomer,[12] H.S. Ng,[2] A.J. Noble,[16,5] E.B. Norman,[8] V.M. Novikov,[5] M. O'Neill,[5] C.E. Okada,[8] R.W. Ollerhead,[6] M. Omori,[11] J.L. Orrell,[17] S.M. Oser,[12] A.W.P. Poon,[8,17,2,9] T.J. Radcliffe,[14] A. Roberge,[7] B.C. Robertson,[14] R.G.H. Robertson,[17,9] S.S.E. Rosendahl,[8] J.K. Rowley,[3] V.L. Rusu,[12] E. Saettler,[7] K.K. Schaffer,[17] M.H. Schwendener,[7] A. Schülke,[8] H. Seifert,[7,17,9] M. Shatkay,[5] J.J. Simpson,[6] C.J. Sims,[11] D. Sinclair,[5] P. Skensved,[14] A.R. Smith,[8] M.W.E. Smith,[17] T. Spreitzer,[12] N. Starinsky,[5] T.D. Steiger,[17] R.G. Stokstad,[8] L.C. Stonehill,[17] R.S. Storey,[10,†] B. Sur,[1,14] R. Tafirout,[7] N. Tagg,[6,11] N.W. Tanner,[11] R.K. Taplin,[11] M. Thorman,[11] P.M. Thornewell,[11] P.T. Trent,[11] Y.I. Tserkovnyak,[2] R. Van Berg,[12] R.G. Van de Water,[9,12] C.J. Virtue,[7] C.E. Waltham,[2] J.-X. Wang,[6] D.L. Wark,[15,11,9] N. West,[11] J.B. Wilhelmy,[9] J.F. Wilkerson,[17,9] J.R. Wilson,[11] P. Wittich,[12] J.M. Wouters,[9] and M. Yeh[3]

(SNO Collaboration)

[1] *Atomic Energy of Canada, Limited, Chalk River Laboratories, Chalk River, ON K0J 1J0, Canada*
[2] *Department of Physics and Astronomy, University of British Columbia, Vancouver, BC V6T 1Z1 Canada*
[3] *Chemistry Department, Brookhaven National Laboratory, Upton, NY 11973-5000*
[4] *Department of Physics, University of California, Irvine, CA 92717*
[5] *Carleton University, Ottawa, Ontario K1S 5B6 Canada*
[6] *Physics Department, University of Guelph, Guelph, Ontario N1G 2W1 Canada*
[7] *Department of Physics and Astronomy, Laurentian University, Sudbury, Ontario P3E 2C6 Canada*
[8] *Institute for Nuclear and Particle Astrophysics and Nuclear Science Division, Lawrence Berkeley National Laboratory, Berkeley, CA 94720*
[9] *Los Alamos National Laboratory, Los Alamos, NM 87545*
[10] *National Research Council of Canada, Ottawa, ON K1A 0R6, Canada*
[11] *Department of Physics, University of Oxford, Denys Wilkinson Building, Keble Road, Oxford, OX1 3RH, UK*
[12] *Department of Physics and Astronomy, University of Pennsylvania, Philadelphia, PA 19104-6396*
[13] *Department of Physics, Princeton University, Princeton, NJ 08544*
[14] *Department of Physics, Queen's University, Kingston, Ontario K7L 3N6 Canada*
[15] *Rutherford Appleton Laboratory, Chilton, Didcot, Oxon, OX11 0QX, and University of Sussex, Physics and Astronomy Department, Brighton BN1 9QH, UK*
[16] *TRIUMF, 4004 Wesbrook Mall, Vancouver, BC V6T 2A3, Canada*
[17] *Center for Experimental Nuclear Physics and Astrophysics, and Department of Physics, University of Washington, Seattle, WA 98195*

(Dated: 19 April 2002)

Observations of neutral-current ν interactions on deuterium in the Sudbury Neutrino Observatory are reported. Using the neutral current, elastic scattering, and charged current reactions and assuming the standard ^{8}B shape, the ν_e component of the ^{8}B solar flux is $\phi_e = 1.76^{+0.05}_{-0.05}(\text{stat.})^{+0.09}_{-0.09}$ (syst.) $\times\ 10^6$ cm^{-2}s^{-1} for a kinetic energy threshold of 5 MeV. The non-ν_e component is $\phi_{\mu\tau} = 3.41^{+0.45}_{-0.45}(\text{stat.})^{+0.48}_{-0.45}$ (syst.) $\times\ 10^6$ cm^{-2}s^{-1}, 5.3σ greater than zero, providing strong evidence for solar ν_e flavor transformation. The total flux measured with the NC reaction is $\phi_{\rm NC} = 5.09^{+0.44}_{-0.43}(\text{stat.})^{+0.46}_{-0.43}$ (syst.) $\times 10^6$ cm^{-2}s^{-1}, consistent with solar models.

PACS numbers: 26.65.+t, 14.60.Pq, 13.15.+g, 95.85.Ry

The Sudbury Neutrino Observatory (SNO) detects ^{8}B solar neutrinos through the reactions:

$$\begin{array}{llll} \nu_e + \mathrm{d} & \rightarrow & \mathrm{p} + \mathrm{p} + \mathrm{e}^- & \text{(CC)}, \\ \nu_x + \mathrm{d} & \rightarrow & \mathrm{p} + \mathrm{n} + \nu_x & \text{(NC)}, \\ \nu_x + \mathrm{e}^- & \rightarrow & \nu_x + e^- & \text{(ES)}. \end{array}$$

The charged current reaction (CC) is sensitive exclusively to electron-type neutrinos, while the neutral current reaction (NC) is equally sensitive to all active neutrino flavors ($x = e, \mu, \tau$). The elastic scattering reaction (ES) is sensitive to all flavors as well, but with reduced sensitivity to ν_μ and ν_τ. Sensitivity to these three reactions allows SNO to determine the electron and non-electron active neutrino components of the solar flux [1]. The CC and ES reaction results have recently been presented [2]. This Letter presents the first NC results and updated CC and ES results from SNO.

SNO [3] is a water Cherenkov detector located at a depth of 6010 m of water equivalent in the INCO, Ltd. Creighton mine near Sudbury, Ontario, Canada. The detector uses ultra-pure heavy water contained in a transparent acrylic spherical shell 12 m in diameter to detect solar neutrinos. Cherenkov photons generated in the heavy water are detected by 9456 photomultiplier tubes (PMTs) mounted on a stainless steel geodesic sphere 17.8 m in diameter. The geodesic sphere is immersed in ultra-pure light water to provide shielding from radioactivity in both the PMT array and the cavity rock.

The data reported here were recorded between Nov. 2, 1999 and May 28, 2001 and represent a total of 306.4 live days, spanning the entire first phase of the experiment, in which only D_2O was present in the sensitive volume. The analysis procedure was similar to that described in [2]. PMT times and hit patterns were used to reconstruct event vertices and directions and to assign to each event a most probable kinetic energy, $T_{\rm eff}$. The total flux of active ^{8}B solar neutrinos with energies greater than 2.2 MeV (the NC reaction threshold) was measured with the NC signal (Cherenkov photons resulting from the 6.25 MeV γ ray from neutron capture on deuterium.) The analysis threshold was $T_{\rm eff} \geq 5$ MeV, providing sensitivity to neutrons from the NC reaction. Above this energy threshold, there were contributions from CC events in the D_2O, ES events in the D_2O and H_2O, capture of neutrons (both from the NC reaction and backgrounds), and low energy Cherenkov background events.

A fiducial volume was defined to only accept events which had reconstructed vertices within 550 cm from the detector center to reduce external backgrounds and systematic uncertainties associated with optics and event reconstruction near the acrylic vessel. The neutron response and systematic uncertainty was calibrated with a ^{252}Cf source. The deduced efficiency for neutron captures on deuterium is $29.9 \pm 1.1\%$ for a uniform source of neutrons in the D_2O. The neutron detection efficiency within the fiducial volume and above the energy threshold is 14.4%. The energy calibration was updated from [2] with the ^{16}N calibration source [4] data and Monte Carlo calculations. The energy response for electrons, updated for the lower analysis threshold, was characterized as a Gaussian function with resolution $\sigma_T = -0.0684 + 0.331\sqrt{T_e} + 0.0425 T_e$, where T_e is the true electron kinetic energy in MeV. The energy scale uncertainty is 1.2%.

The primary backgrounds to the NC signal are due to low levels of uranium and thorium decay chain daughters (^{214}Bi and ^{208}Tl) in the detector materials. These activities generate free neutrons in the D_2O, from deuteron photodisintegration (pd), and low energy Cherenkov events. *Ex-situ* assays and *in-situ* analysis of the low energy (4 − 4.5 MeV) Cherenkov signal region provide independent uranium and thorium photodisintegration background measurements.

Two *ex situ* assay techniques were employed to determine average levels of uranium and thorium in water. Radium ions were directly extracted from the water onto either MnO_x or hydrous Ti oxide (HTiO) ion exchange media. Radon daughters in the U and Th chains were subsequently released, identified by α spectroscopy, or the radium was concentrated and the number of decay daughter β-α coincidences determined. Typical assays circulated approximately 400 tonnes of water through the extraction media. These techniques provide isotopic identification of the decay daughters and contamination levels in the assayed water volumes, presented in Fig. 1 (a). Secular equilibrium in the U decay chain was broken by the ingress of long-lived (3.8 day half-life) ^{222}Rn in the experiment. Measurements of this background were made by periodically extracting and cryogenically concentrating ^{222}Rn from water degassers. Radon from several tonne assays was subsequently counted in ZnS(Ag) scintillation cells [5]. The Radon results are presented (as mass fractions in g(U)/g(D_2O)) in Fig. 1(b).

Independent measurements of U and Th decay chains were made by analyzing Cherenkov light produced by the radioactive decays. The β and β-γ decays from the U and Th chains dominate the low energy monitoring window. Events in this window monitor γ rays that produce photodisintegration in these chains ($E_\gamma > 2.2$ MeV). Cherenkov events fitted within 450 cm from the detector center and extracted from the neutrino data set provide a time-integrated measure of these backgrounds over the same time period and within the fiducial volume of the neutrino analysis. Statistical separation of *in situ* Tl and Bi events was obtained by analyzing the Cherenkov signal isotropy. Tl decays always result in a β and a 2.614 MeV γ, while in this energy window Bi decays are dominated by decays with only a β, and produce, on average, more anisotropic hit patterns.

Results from the *ex situ* and *in situ* methods are consistent with each other as shown on the right hand side of Figs. 1(a) and 1(b). For the ^{232}Th chain, the weighted mean (including additional sampling systematic uncertainty) of the two determinations was used for the analysis. The ^{238}U chain activity is dominated by Rn ingress which is highly time dependent. Therefore the *in-situ* determination was used for this activity as it provides the appropriate time weighting. The average rate of background neutron production from activities in the D_2O region is 1.0 ± 0.2 neutrons per day, leading to 44^{+8}_{-9} detected background events. The production rate from external activities is $1.3^{+0.4}_{-0.5}$ neutrons per day, which leads to 27 ± 8 background events since the neutron capture efficiency is reduced for neutrons born near the heavy water boundary. The total photodisintegration background corresponds to approximately 12% of the number of NC neutrons predicted by the standard solar model from ^{8}B neutrinos.

Low energy backgrounds from Cherenkov events in the signal region were evaluated by using acrylic encapsulated sources of U and Th deployed throughout the detector volume and by Monte Carlo calculations. Probability density functions (pdfs) in reconstructed vertex radius derived from U and Th calibration data were used to determine the number of background Cherenkov events from external regions which either entered or misreconstructed into the fiducial volume. Cherenkov event backgrounds from activities in the D_2O were evaluated with Monte Carlo calculations.

Table I shows the number of photodisintegration and Cherenkov background events (including systematic uncertainties) due to activity in the D_2O (internal region), acrylic vessel (AV), H_2O (external region), and PMT array. Other sources of free neutrons in the D_2O region are cosmic ray events and atmospheric neutrinos. To reduce these backgrounds, an additional neutron background cut imposed a 250-ms deadtime (in software) following every event in which the total number of PMTs which registered a hit was greater than 60. The number of remaining NC atmospheric neutrino events and background events generated by sub-Cherenkov threshold muons is estimated to be small, as shown in Table I.

The data recorded during the pure D_2O detector phase are shown in Figure 2. These data have been analyzed using the same data reduction described in [2], with the addition of the new neutron background cut, yielding

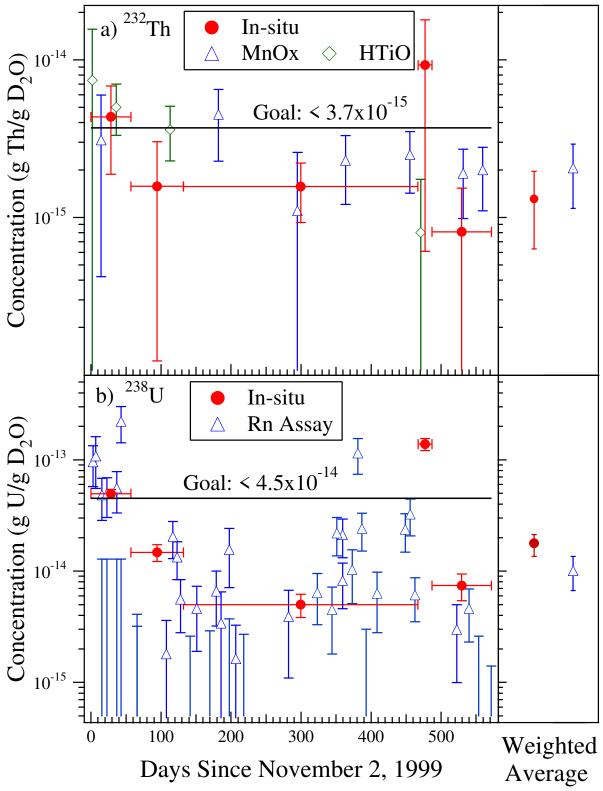

FIG. 1: Thorium (a) and uranium (b) backgrounds (equivalent equilibrium concentrations) in the D_2O deduced by *in situ* and *ex situ* techniques. The MnO_x and HTiO radiochemical assay results, the Rn assay results, and the *in situ* Cherenkov signal determination of the backgrounds are presented for the period of this analysis on the left-hand side of frames (a) and (b). The right-hand side shows time-integrated averages including an additional sampling systematic uncertainty for the *ex situ* measurement.

TABLE I: Neutron and Cherenkov background events.

Source	Events
D_2O photodisintegration	44^{+8}_{-9}
H_2O + AV photodisintegration	27^{+8}_{-8}
Atmospheric ν's and sub-Cherenkov threshold μ's	4 ± 1
Fission	$\ll 1$
^{2}H(α,α)pn	2 ± 0.4
^{17}O$(\alpha$,n)	$\ll 1$
Terrestrial and reactor $\bar{\nu}$'s	1^{+3}_{-1}
External neutrons	$\ll 1$
Total neutron background	78 ± 12
D_2O Cherenkov	20^{+13}_{-6}
H_2O Cherenkov	3^{+4}_{-3}
AV Cherenkov	6^{+3}_{-6}
PMT Cherenkov	16^{+11}_{-8}
Total Cherenkov background	45^{+18}_{-12}

TABLE II: Systematic uncertainties on fluxes. The experimental uncertainty for ES (not shown) is -4.8,+5.0 percent. † denotes CC vs NC anti-correlation.

Source	CC Uncert. (percent)	NC Uncert. (percent)	$\phi_{\mu\tau}$ Uncert. (percent)
Energy scale †	-4.2,+4.3	-6.2,+6.1	-10.4,+10.3
Energy resolution †	-0.9,+0.0	-0.0,+4.4	-0.0,+6.8
Energy non-linearity †	±0.1	±0.4	±0.6
Vertex resolution †	±0.0	±0.1	±0.2
Vertex accuracy	-2.8,+2.9	±1.8	±1.4
Angular resolution	-0.2,+0.2	-0.3,+0.3	-0.3,+0.3
Internal source pd †	±0.0	-1.5,+1.6	-2.0,+2.2
External source pd	±0.1	-1.0,+1.0	±1.4
D_2O Cherenkov †	-0.1,+0.2	-2.6,+1.2	-3.7,+1.7
H_2O Cherenkov	±0.0	-0.2,+0.4	-0.2,+0.6
AV Cherenkov	±0.0	-0.2,+0.2	-0.3,+0.3
PMT Cherenkov †	±0.1	-2.1,+1.6	-3.0,+2.2
Neutron capture	±0.0	-4.0,+3.6	-5.8,+5.2
Cut acceptance	-0.2,+0.4	-0.2,+0.4	-0.2,+0.4
Experimental uncertainty	-5.2,+5.2	-8.5,+9.1	-13.2,+14.1
Cross section [7]	±1.8	±1.3	±1.4

2928 events in the energy region selected for analysis, 5 to 20 MeV. Fig. 2(a) shows the distribution of selected events in the cosine of the angle between the Cherenkov event direction and the direction from the sun ($\cos\theta_\odot$) for the analysis threshold of $T_{\rm eff}\geq$ 5 MeV and fiducial volume selection of $R \leq 550$ cm, where R is the reconstructed event radius. Fig. 2(b) shows the distribution of events in the volume-weighted radial variable $(R/R_{\rm AV})^3$, where $R_{\rm AV} = 600$ cm is the radius of the acrylic vessel. Figure 2(c) shows the kinetic energy spectrum of the selected events.

In order to test the null hypothesis, the assumption that there are only electron neutrinos in the solar neutrino flux, the data are resolved into contributions from CC, ES, and NC events above threshold using pdfs in $T_{\rm eff}$, $\cos\theta_\odot$, and $(R/R_{\rm AV})^3$, derived from Monte Carlo calculations generated assuming no flavor transformation and the standard ^{8}B spectral shape [6]. Background event pdfs are included in the analysis with fixed amplitudes determined by the background calibration. The extended maximum likelihood method used in the signal decomposition yields $1967.7^{+61.9}_{-60.9}$ CC events, $263.6^{+26.4}_{-25.6}$ ES events, and $576.5^{+49.5}_{-48.9}$ NC events [12], where only statistical uncertainties are given. Systematic uncertainties on fluxes derived by repeating the signal decomposition with perturbed pdfs (constrained by calibration data) are shown in Table II.

Normalized to the integrated rates above the kinetic energy threshold of $T_{\rm eff}\geq$ 5 MeV, the flux of ^{8}B neutrinos measured with each reaction in SNO, assuming the standard spectrum shape [6] is (all fluxes are presented in units of 10^6 cm^{-2}s^{-1}):

$$\phi^{\rm SNO}_{\rm CC} = 1.76^{+0.06}_{-0.05}({\rm stat.})^{+0.09}_{-0.09}\ ({\rm syst.})$$
$$\phi^{\rm SNO}_{\rm ES} = 2.39^{+0.24}_{-0.23}({\rm stat.})^{+0.12}_{-0.12}\ ({\rm syst.})$$
$$\phi^{\rm SNO}_{\rm NC} = 5.09^{+0.44}_{-0.43}({\rm stat.})^{+0.46}_{-0.43}\ ({\rm syst.}).$$

Electron neutrino cross sections are used to calculate all

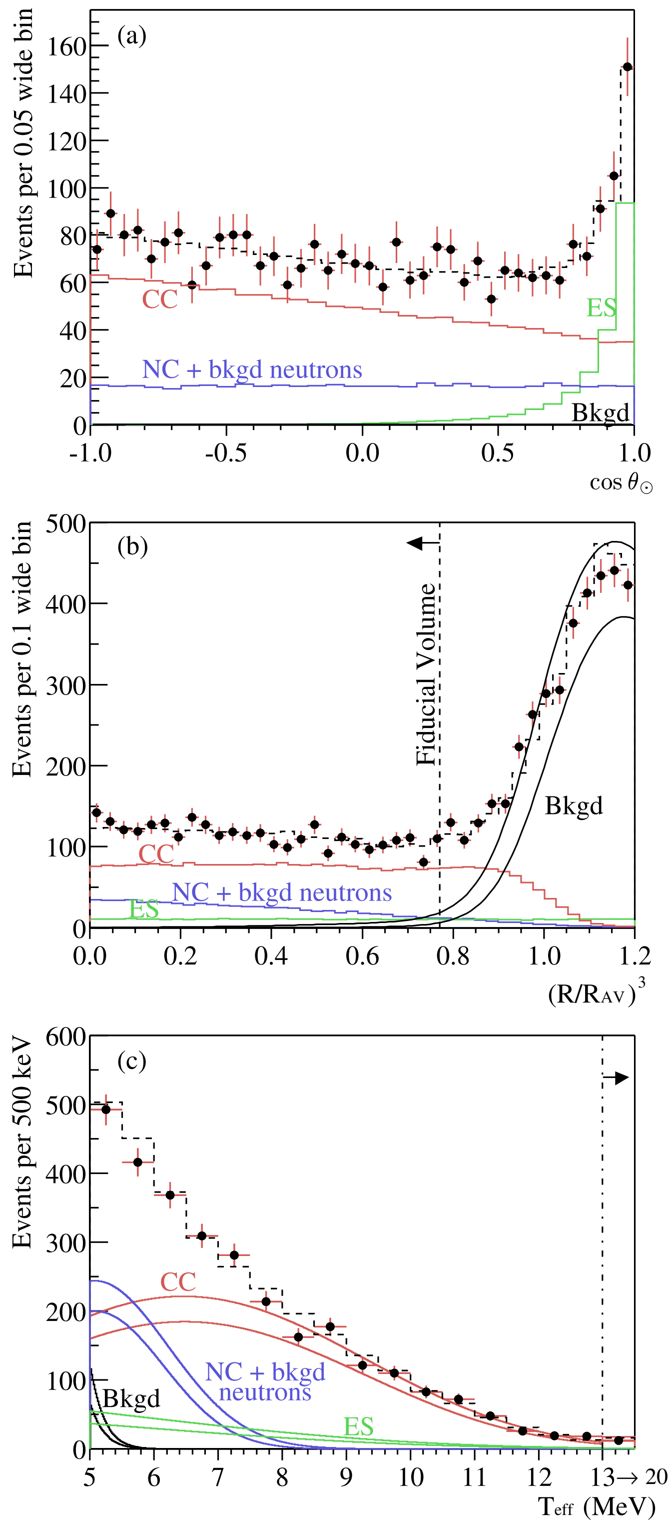

FIG. 2: (a) Distribution of $\cos\theta_\odot$ for $R \leq 550$ cm. (b) Distribution of the volume weighted radial variable $(R/R_{\rm AV})^3$. (c) Kinetic energy for $R \leq 550$ cm. Also shown are the Monte Carlo predictions for CC, ES and NC + bkgd neutron events scaled to the fit results, and the calculated spectrum of Cherenkov background (Bkgd) events. The dashed lines represent the summed components, and the bands show $\pm1\sigma$ uncertainties. All distributions are for events with $T_{\rm eff}\geq$5 MeV.

fluxes. The CC and ES results reported here are consistent with the earlier SNO results [2] for $T_{\rm eff}\geq 6.75$ MeV. The excess of the NC flux over the CC and ES fluxes implies neutrino flavor transformations.

A simple change of variables resolves the data directly into electron (ϕ_e) and non-electron ($\phi_{\mu\tau}$) components [13],

$$\phi_e = 1.76^{+0.05}_{-0.05}(\text{stat.})^{+0.09}_{-0.09}\ (\text{syst.})$$
$$\phi_{\mu\tau} = 3.41^{+0.45}_{-0.45}(\text{stat.})^{+0.48}_{-0.45}\ (\text{syst.})$$

assuming the standard ^{8}B shape. Combining the statistical and systematic uncertainties in quadrature, $\phi_{\mu\tau}$ is $3.41^{+0.66}_{-0.64}$, which is 5.3σ above zero, providing strong evidence for flavor transformation consistent with neutrino oscillations [8, 9]. Adding the Super-Kamiokande ES measurement of the ^{8}B flux [10] $\phi_{\rm ES}^{\rm SK} = 2.32 \pm 0.03(\text{stat.})^{+0.08}_{-0.07}$ (syst.) as an additional constraint, we find $\phi_{\mu\tau} = 3.45^{+0.65}_{-0.62}$, which is 5.5σ above zero. Figure 3 shows the flux of non-electron flavor active neutrinos vs the flux of electron neutrinos deduced from the SNO data. The three bands represent the one standard deviation measurements of the CC, ES, and NC rates. The error ellipses represent the 68%, 95%, and 99% joint probability contours for ϕ_e and $\phi_{\mu\tau}$.

Removing the constraint that the solar neutrino energy spectrum is undistorted, the signal decomposition is repeated using only the $\cos\theta_\odot$ and $(R/R_{\rm AV})^3$ information. The total flux of active ^{8}B neutrinos measured with the NC reaction is

$$\phi_{\rm NC}^{\rm SNO} = 6.42^{+1.57}_{-1.57}(\text{stat.})^{+0.55}_{-0.58}\ (\text{syst.})$$

which is in agreement with the shape constrained value above and with the standard solar model prediction [11] for ^{8}B, $\phi_{\rm SSM} = 5.05^{+1.01}_{-0.81}$.

In summary, the results presented here are the first direct measurement of the total flux of active ^{8}B neutrinos arriving from the sun and provide strong evidence for neutrino flavor transformation. The CC and ES reaction rates are consistent with the earlier results [2] and with the NC reaction rate under the hypothesis of flavor transformation. The total flux of ^{8}B neutrinos measured with the NC reaction is in agreement with the SSM prediction.

This research was supported by: Canada: NSERC, Industry Canada, NRC, Northern Ontario Heritage Fund Corporation, Inco, AECL, Ontario Power Generation; US: Dept. of Energy; UK: PPARC. We thank the SNO technical staff for their strong contributions.

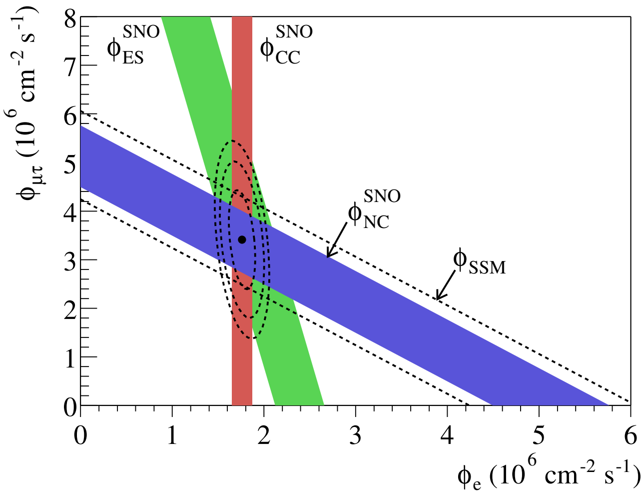

FIG. 3: Flux of ^{8}B solar neutrinos which are μ or τ flavor vs flux of electron neutrinos deduced from the three neutrino reactions in SNO. The diagonal bands show the total ^{8}B flux as predicted by the SSM [11] (dashed lines) and that measured with the NC reaction in SNO (solid band). The intercepts of these bands with the axes represent the $\pm 1\sigma$ errors. The bands intersect at the fit values for ϕ_e and $\phi_{\mu\tau}$, indicating that the combined flux results are consistent with neutrino flavor transformation assuming no distortion in the ^{8}B neutrino energy spectrum.

* Permanent Address: Birkbeck College, University of London, Malet Road, London WC1E 7HX, UK
† Deceased

[1] H. Chen, Phys. Rev. Lett. **55**, 1534 (1985).
[2] Q.R. Ahmad *et al.*, Phys. Rev. Lett. **87**, 071301 (2001).
[3] The SNO collaboration, Nucl. Instr. and Meth. **A449**, 172 (2000).
[4] M. R. Dragowsky *et al.*, Nucl. Instr. and Meth. **A481**, 284 (2002).
[5] M.-Q. Liu, H.W. Lee, and A.B. McDonald, Nucl. Inst. Meth. **A329**, 291 (1993).
[6] C. E. Ortiz *et al.*, Phys. Rev. Lett. **85**, 2909 (2000).
[7] Cross section uncertainty includes g_A uncertainty (0.6%), difference between NSGK (S. Nakamura, T. Sato, V. Gudkov and K. Kubodera, Phys. Rev. **C63** (2001) 034617) and BCK (M. Butler, J.-W. Chen and X. Kong, Phys. Rev. **C63** (2001) 035501) in SNO's calculations (0.6%), radiative correction uncertainties (0.3% for CC, 0.1% for NC, A. Kurylov, M. J. Ramsey-Musolf and P. Vogel, Phys. Rev. **C65** (2002) 055501), uncertainty associated with neglect of real photons in SNO (0.7% for CC), and theoretical cross section uncertainty (1%, S. Nakamura *et al.*, `arXiv:nucl-th/0201062`, (to be published)).
[8] Z. Maki, N. Nakagawa, and S. Sakata, Prog. Theor. Phys. **28**, 870 (1962).
[9] V. Gribov and B. Pontecorvo, Phys. Lett. **B28**, 493 (1969).
[10] S. Fukuda *et al.*, Phys. Rev. Lett. **86**, 5651 (2001).
[11] John N. Bahcall, M.H. Pinsonneault, and Sarbani Basu, Astrophys. J. **555**, 990 (2001).
[12] We note that this rate of neutron events also leads to a lower bound on the proton lifetime for "invisible" modes (based on the free neutron that would be left in deuterium (V.I. Tretyak and Yu.G. Zdesenko, Phys. Lett. **B505**, 59 (2001)) in excess of 10^{28} years, approximately

3 orders of magnitude more restrictive than previous limits (J. Evans and R. Steinberg, Science, **197**, 989 (1977).) The possible contribution of this mechanism to the solar neutrino NC background is ignored.

[13] This change of variables allows a direct test of the null hypothesis of no flavor transformation ($\phi_{\mu\tau} = 0$) without requiring calculation of the CC, ES, and NC signal correlations.